Journal of Dentistry 132 (2023) 104470

Contents lists available at ScienceDirect

Journal of Dentistry

journal homepage: www.elsevier.com/locate/jdent

'Thermo-mechanical behavior of alternative material combinations for full-arch implant-supported hybrid prostheses with short cantilevers'

Evelina Haroyan-Darbinyan [a], Marta Romeo-Rubio [a], Jaime Del Río-Highsmith [a], Christopher D. Lynch [b], Raquel Castillo-Oyagüe [a,*]

[a] Faculty of Dentistry, Complutense University of Madrid (U.C.M.), Madrid, Spain
[b] University Dental School & Hospital/ University College Cork, Wilton, Cork, Ireland

ARTICLE INFO

Keywords:
Full-arch implant-supported hybrid prosthesis
Short cantilever
Prosthetic mesostructure
Carbon fiber
Cobalt-chromium
Resin coating

ABSTRACT

Objectives: To compare the fracture resistance (FR) of three combinations of materials for full-arch maxillary implant-supported hybrid prostheses (HPs) with short cantilevers (≤ 10 mm).
Methods: Maxillary HPs were fabricated and classified as follows (n = 5 each): Group-1 (CC-A, *control*): acrylic-resin-veneered Co-Cr frameworks; Group-2 (CF-A): acrylic-resin-veneered carbon-fiber mesostructures; and Group-3 (CF-R): composite-resin-veneered carbon-fiber frames. Specimens were thermal-cycled (5,000 cycles; 5 °C–55 °C; dwell time: 30 s). Vertical loads were applied until failure, first at the 10-mm-long cantilever (LC), and, afterwards, at the anterior region (AR), using a universal testing machine (crosshead speed: 0.05 mm/s). The fracture pattern was assessed by stereomicroscope and SEM. The one-way ANOVA, the Bonferroni, and the independent samples t tests, were run (α= 0.05).
Results: At LC, CF-A, and CC-A samples exhibited the highest FR values (p< 0.001), showing no differences to each other. At AR, CC-A specimens recorded the highest FR, followed by CF-A samples (p< 0.001). CF-R HPs displayed the lowest FR at both locations (p< 0.001). The only group with differences between the tested sites was the CC-A, the AR being more resistant (p< 0.001). Most CC-A and CF-A HPs failed cohesively. CF-R prostheses mainly failed adhesively.
Conclusions: Maxillary HPs with short cantilevers (≤ 10 mm) made of Co-Cr or carbon-fiber veneered with acrylic resin demonstrated an adequate mechanical resistance (> 900 N).
Clinical significance: For maxillary HPs with cantilevers up to 10 mm, acrylic-veneered carbon- fiber mesostructures may be recommended, whereas coating carbon-fiber frames with composite resin seems not suitable.

1. Introduction

Full-arch implant-supported hybrid prostheses (HPs) have become an effective treatment option for those edentate patients with high available prosthetic space due to severe alveolar bone resorption [1–3]. Given that HP fixtures are mainly placed in the anterior region of the maxilla and/or mandible, such a design results in bilateral cantilevered framework segments [4].

Loads on distal extensions may create a high potential for bending due to a hinging effect of the restorations [5]. This yields points of stress around the crestal bone of the distal implants [6], which seem to increase with the cantilever length [7]. Moreover, prosthetic failures due to screws loosening and/or fracturing, debonding of the acrylic veneering, and detachment of artificial teeth are still the most frequent complications related to HPs. Notwithstanding the lack of consensus concerning the maximum tolerated cantilever span [8], several variables have been suggested in this regard, such as the anterior-posterior spread [9], the number of implants supporting the rehabilitation [10], the type and magnitude of the occlusal loads [11], the arch shape [12], and the combination of prosthodontic materials [13].

On the one hand, the development of biocompatible metal-free materials such as carbon fibers [14,15], judged to display adequate stiffness [16,17] and proper adhesion to acrylic resin [18], have been marketed for constructing prosthetic structures. However, very few investigations have addressed their mechanical behavior [15,16,18], and even fewer concern cantilevers [14].

* Corresponding author at: Department of Conservative & Prosthetic Dentistry, Faculty of Dentistry, Complutense University of Madrid (U.C.M.), Pza. Ramón y Cajal s/n, 28040, Madrid, Spain.
E-mail address: raquel.castillo@ucm.es (R. Castillo-Oyagüe).

https://doi.org/10.1016/j.jdent.2023.104470
Received 25 November 2022; Received in revised form 27 January 2023; Accepted 2 February 2023
Available online 24 February 2023

On the other hand, distal extensions should be as short as possible [19], especially in the maxilla, due to its diminished bone-loading capacity [20]. Even though maximum cantilever lengths of 15–20 mm in the mandible [21,22], and of 10–15 mm in the maxilla [22–24] have traditionally been recommended, we tested maxillary HPs with 10-mm extensions, as longer cantilevers have been discouraged for the upper jaw by most authors [21,22]. This value also coincides with the average mesiodistal length of the maxillary first molar [25], which may be set instead of the second premolar to improve the masticatory function [26,27]. The shortened dental-arch concept (SDA) may thus represent an alternative treatment option [28–30] to reduce the deflection of the restoration and the stress on the implant/bone interfaces caused by the load on HPs' cantilevers [31].

To date, few studies have addressed fracture resistance in maxillary HPs [16,32], and none have compared the materials and manufacturing techniques analysed in our experiment for cantilevers and intermediate sectors. Hence, this *in vitro* study was intended to determine the best combination of mesostructure and suprastructure materials for fabricating resistant full-arch maxillary HPs with short cantilevers (≤10 mm). As a clinical reference, the FR values recorded in the study groups were compared with the empirically acceptable limit of 900 N [14,33].

The null hypothesis tested was that maxillary HPs made of acrylic-coated cobalt-chromium ('gold standard'), carbon fiber veneered with acrylic resin, and carbon fiber covered with composite resin show similar FR and fracture patterns regardless of the location tested (10-mm-long cantilever *vs.* anterior region).

2. Materials and methods

2.1. Sample size calculation

The sample size was calculated with the nQuery Sample Size Software® (v. 7.0, Statsols®, Boston, MA, US) based on the FR means and standard deviations of five HPs per experimental group. The pilot study was validated as the main research. The minimum necessary number of specimens per group to meet the desired statistical constraints (power of 95% and significance level of α= 0.05) [34] was three. Nonetheless, to obtain more accurate data, the five prostheses per group were maintained [14,16,35,36].

2.2. Design and fabrication of the samples

Fifteen maxillary full-arch implant-supported cantilevered hybrid prostheses (HPs) were CAD/CAM fabricated for this *in vitro* study. According to the combination of framework (mesostructure) and coating or veneering (suprastructure) materials, the restorations were assigned to the next groups (n = 5 each): Group-1 (CC-A, *control*): Acrylic-resin-veneered cobalt-chromium HPs; Group-2 (CF-A): Acrylic-resin-coated carbon-fiber HPs; and Group-3 (CF-R): composite-resin-veneered carbon-fiber HPs. An experienced prosthetic technician fabricated all the HPs.

Five cylindrical dental implants were embedded in a stainless-steel machined support. The implants (Nobel Biocare®, Gothenburg, Sweden) had an external hexagon connection, a 3.75-mm-wide platform, a length of 10 mm, and a diameter (Ø) of 4.1 mm; and were placed in the 1.4, 1.2, 1.1, 2.2, and 2.4 arch positions.

The metallic model was digitized with an extraoral laboratory scanner (3Shape® D2000 Dental System, Copenhagen, Denmark). A computer-aided designed (CAD) frame (Fig. 1) for maxillary HPs was saved as an STL file and sent to a milling unit (VHF-S2, VHF, Ammerbach, Germany). For the control group, five structures were machined from cobalt-chromium (Co-Cr) disks (Imes-icore GmbH®, Eiterfeld, Germany). For the experimental groups, ten frameworks were milled from 100% carbon-fiber disks (Micromedica®, Robbio, Italy), which were randomly assigned to the Groups 2 and 3 (n = 5 each). All the structures were cleaned with water and gently air-dried.

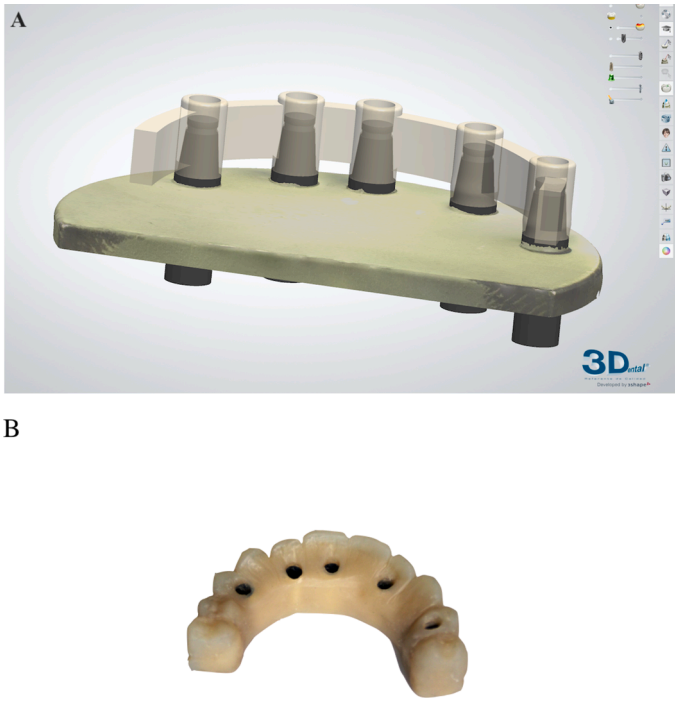

Fig. 1. A: Computer-aided design (CAD) of the mesostructure used to fabricate all the specimens. **B:** Experimental sample consisting of a maxillary hybrid prosthesis that simulates a shortened dental arch, made, in this case, of carbon fiber coated with composite resin (CF-R_5).

To ensure the exact transfer of the prosthesis' morphology to all HPs, a wax pattern of the suprastructure (Bader®, Nigrán, Pontevedra, Spain) was hand fabricated, and a silicon mold was prepared from the mock-up (Glass Silicon®, Micromedica®, Robbio, Italy).

The color of the Co-Cr samples was masked with a film of metal bonding (Link®, Ivoclar-Vivadent®, Schaän, Liechtenstein) and two layers of wash opaque paste (Opaquer Nexco®, Gingiva Opaquer®, Ivoclar-Vivadent®, Schaän, Liechtenstein). The darkness of the carbon-fiber frames was camouflaged with adhesive (BioxFill®, Micromedica®, Robbio, Italy) and two layers of wash opaque material (BioxFill® Opaquer Medium, Micromedica®, Robbio, Italy). All the structures were light-cured for 3 min after the application of the adhesive and the opaquer (HiLite® Power, Heraeus, Hanau, Germany).

In both the CC-A and CF-A groups, the artificial teeth were inserted into their respective positions within the silicone mold. For the construction of the prosthetic gum, heat-polymerising acrylic resin (Paladon 65 Pink®, Kulzer®, Tokyo, Japan) was poured in the muffle with each structure, and was processed in a curing unit for 15 min, at 55 °C (131°F), and 2 bars of pressure (Mestra 030,420®, Mestraitua S.L, Bilbao, Spain). Any acrylic excess and irregularity on the edges were adjusted with handpiece burs. The polish was completed using an electropolishing machine with a cotton brush (Mestra®, Mestraitua S.L, Bilbao, Spain). In the CF-R group, the denture teeth and the soft tissues were built-up with composite resin (Nexco® A2, Ivoclar-Vivadent®, Schaän, Liechtenstein) by means of 2-mm-increments inside the silicone mold. Each composite film was light-cured for 40 s (HiLite® Power, Heraeus, Hanau, Germany).

The connections at the mesostructure/implant interfaces were finally sandblasted with 100 μm Ø aluminum oxide (Al_2O_3) particles (pressure: 1 kg, distance: 5 cm), and were steam cleaned. The connections of the CC-A samples were then bonded to the frameworks using a metal-adhesive primer (Monobond Plus®, Ivoclar-Vivadent®, Schaän, Liechtenstein) and a self-cure luting agent (Multilink Hybrid Abutment®, Ivoclar-Vivadent®, Schaän, Liechtenstein).

The connections of the CF-A and CF-R specimens were luted to the

carbon-fiber mesostructures with a compatible cement (Carbobloc®, Micromedica®, Robbio, Italy).

2.3. Artificial aging

Ten litres of artificial saliva were formulated in the chemical laboratory of the Faculty of Dentistry of the Complutense University of Madrid (U.C.M., Spain), with this composition (g/L): NaCl (0.400); KCl (0.400); $CaCl_2 2H_2O$ (0.906); $NaH_2PO_4 2H_2O$ (0.069); $Na_2S 9H_2O$ (0.005); and urea (1.000). The aging protocol for biomaterials defined in the normative of the International Organization for standardisation (ISO) TR 11,405:2015 was rigorously followed. The implant prostheses were submitted to thermal cycling in a custom-built thermocycling device. The samples underwent 5000 cycles in an artificial saliva medium (pH= 7), with a dwell time of 30 s, a transfer time of 2 s between consecutive cycles, and temperatures ranging from 5 °C to 55 °C (41°F to 98°F). This aging procedure would correspond to 1 year of clinical service [14,37].

2.4. Mechanical testing

After thermal cycling, the specimens remained stored in artificial saliva at 37 °C (98.6°F). Before loading, the HPs were dried and codified with three capital letters (two for the mesostructure material, script, and one letter for the suprastructure material). The prostheses were randomly differentiated by subscript numbers from 1 to 5 within each group.

All the samples were submitted to a flexural load in a universal testing machine (ZwickRoell® Z 2.5 TN, Ulm, Germany) at the Laboratory of Euroortodoncia, S.L. (Alcorcón, Madrid, Spain), with the collaboration of an expert engineer. As described elsewhere [14], the 13-mm-long extensions of our specimens had previously been loaded until failure by means of a standardized method (MTS Insight® 45, Eden Prairie, US). Such test was focussed on the resistance of cantilevers longer than those recommended. The 13-mm-long cantilevers of carbon-fiber HPs demonstrated clinically unacceptable FR values regardless of the veneering material (acrylic or composite resin) [14], Hence, we considered it interesting to analyze the FR of the left 10-mm-long extensions, which resembled a shortened dental arch with a cantilevered molar [38]. Furthermore, the FR of the 10-mm-long extensions was compared with that of the anterior region (AR) in the present study.

Before loading, we verified the absence of failures or imperfections at the LC sites under a stereomicroscope (Leica M80®, Heerbrugg, Switzerland) using 40 × magnifications and a LED light source (CLS 100 Leica®, Heerbrugg, Switzerland). As we set out to detect the minimum differences with the highest possible reliability, we chose a universal testing machine with twice the accuracy and almost twice as precise to that used in the first experiment [14]. Thus, the equipment utilized in the current study (ZwickRoell® Z 2.5) has a maximum capacity of 2.5 kN, an accuracy of ± 0.25% of the force exerted (*vs.* ± 0.5% of the MTS Insight® 45), and a speed precision of ± 0.0277 μm (*vs.* ± 0.05 μm of the MTS Insight® 45). The standard error of the measurement of the bending test was 145.95 (standard deviation at baseline= 390.76; Cronbach's α= 0.8065) at the LC site and 235.42 (standard deviation at baseline= 533.68; Cronbach's α= 0.8054) at the AR site. This means less than 50% of the standard error of the measurement of the bending test carried out at the 13-mm-long cantilevers and sensibly higher Cronbach's α values [14]. Thereby, the measurement parameters were even more refined in the present research. The ZwickRoell® Z 2.5 machine was calibrated by an engineer according to the ISO 7500 and ASTM E4 standards two months before testing.

For the bending experiment, the metallic model with the embedded implants was horizontally oriented and screwed to the plate of the universal testing machine. The hybrid prostheses were first connected to the implant analogs and, then, were seated into the metallic model to ensure the passive fit of the restorations before being load until failure. Each sample was fixed to the implants of the master model throughout all the cemented connections using standard titanium screws (IPD®, Mataró, Barcelona, Spain) that were tightened to 30 Ncm [1] with an electronic torque wrench (Nobel Biocare Torque Controller®, Gothenburg, Sweden).

The flexural load was exerted in two marked locations: first, at the LC, and afterwards, at the AR. At the LC, the vertical load was applied at the mesiodistal midpoint between the posterior implant (2.4) and the end of the 10-mm-long cantilever. At the AR, the load was exerted onto the mesiodistal midpoint between the implants in positions 1.1 and 2.2 (*i.e.,* 5 mm distal to the center of the implant 1.1 and 5 mm mesial to the center of the implant 2.2), always coinciding with the midpoint along the vestibular-lingual dimension.

A Ø 5 mm stainless-steel round-ended cylindrical punch was attached to the load cell and was alternatively adjusted to the LC and AR sites of each prosthesis. A 0.2-mm-thick tin foil (Dentaurum®, Ispringen, Germany) was set between the punch and the occlusal surface of each sample [18,39]. The tin foil was used for the load to be uniformly distributed onto the occlusal surface. This prevented possible perforations caused by excessive stress concentrations [16,40] and fracture patterns far from those clinically expected [39,40]. The interposition of food between the dental arches during chewing was therefore approached [16,39,40].

A vertical force with an initial module of 0.2 N was programmed at a crosshead speed of 0.5 mm/min until the fracture and/or the detachment of the veneering material occurred. The failure initiation was announced by a marked decrease in the stress plot of the loading curve, accompanied by visible and audible signs of cracks. The data obtained were compiled and evaluated using the TestWork® software (MTS®, Eden Prairie, US). The bending test was performed by the same trained operator at room temperature (23.0 ± 1.0 °C, *i.e.,* 73.4 ± 33.8°F) and relative humidity (50 ± 5%) conditions [36].

2.5. Evaluation of the fracture pattern under stereomicroscope and SEM

After the bending test, the failure modes were classified as: 'adhesive' (debonding of the veneering material), 'cohesive' (cracks within the thickness of the suprastructure, with or without chipping), 'mixed' (combination of adhesive and cohesive), and 'complete failure' (total breakage of the framework).

The failure modes were assessed under a stereomicroscope (Leica M80®, Heerbrugg, Switzerland), at 40 × magnifications, using a LED light source (CLS 100 Leica®, Heerbrugg, Switzerland). Images of the fractured areas were taken with the Leica DFC 450® digital camera that was integrated into the magnification equipment (5-megapixel CCD sensor).

Representative surfaces from each group were examined by SEM (JSM-6400®, Jeol®, Tokyo, Japan) at different magnifications (250 ×, 300 × and 500 ×). To avoid possible distortions that may appear in non-conductive specimens, a 10-nm-thick gold film was homogeneously sputtered beforehand onto the fractured surfaces, in a metallizing machine, under vacuum (Quorum Q150R S®, East Sussex, UK). The SEM allowed a 3-D scanning resolution of 4 nm at an accelerating voltage of 20 kV [41]. Given the curvilinear morphology of the HPs, the specimens were fitted onto the customized basis to get the best projection angles with respect to the optical axis of the microscope [36]. A specialized technician, supervised by the authors, metallized the HPs and managed the SEM.

2.6. Statistical analysis

Specific software (SPSS® v28, IBM®, Armonk, NY, US) was utilized for the statistical analysis of the fracture resistance (FR). Descriptive statistics included means, standard deviations, medians, interquartile ranges, and maximum and minimum values in Newton (N).

The Shapiro-Wilk was the normality test chosen, because it has more power to detect the non-normality of small samples [42]. As the data set was consistent with the normal distribution, parametric tests were applied. According to well-established statistical methods used in related research [16,43], the FR data recorded at the LC and AR sites were independently processed. The one-way ANOVA and the *post hoc* Bonferroni pairwise comparison test were run to investigate the differences between the three groups at each location [16]. Within each group, the independent samples *t*-test was used to compare the FR values between both tested sites [43]. A significance level of $\alpha = 0.05$ was considered [41,43].

The failure modes registered at each location were categorized and reported as frequencies in percentages within each study group (qualitative variable) [14].

3. Results

3.1. Fracture load

The specimens were not affected at all by the effects of the artificial aging. Descriptive FR statistics for the LC and AR sites are outlined in Tables 1 and 2, respectively. The spread and centers of the set of FR values registered in each group are shown in Fig. 2, with box and whiskers plots. At the LC, the tested groups yielded significant differences ($p < 0.001$). According to the *post hoc* comparisons, the CF-R prostheses recorded the significantly lowest FR (799.4 ± 93.0 N), whereas the CC-A (1603.6 ± 137.3 N) and CF-A (1546.8 ± 58.0 N) restorations achieved the highest FR with no significant differences to each other (Table 1).

At the AR location, significant differences were evidenced between all groups ($p < 0.001$). The CC-A samples recorded the significantly highest FR values (2148.0 ± 154.2 N), followed by the CF-A restorations (1462.0 ± 131.4 N), which exhibited, in turn, significantly higher FR values than those of the CF-R prostheses (922.4 ± 111.9 N).

All groups exceeded the threshold of 900 N at both tested sites, except the CF-R samples at the LC (Tables1 and 2).

Within each study group, the FR values of the LC and AR locations were compared with each other (Table 3). In the CC-A group, the FR of the AR site was significantly higher than that of the LC ($p < 0.001$). Both tested sites attained statistically comparable FR values within both the CF-A ($p = 0.223$) and the CF-R ($p = 0.095$) groups (Table 3).

3.2. Microscope evaluation and fracture pattern

Representative stereomicroscope (40 ×) and SEM (250 ×, 300 ×, and 500 ×) images of the specimens are displayed in Figs. 3-5. The initiation and propagation of the fracture lines, as well as the superficial fissures, were first evaluated under stereomicroscope at 40 × magnifications. The detached elements and micro-gaps were then explored under SEM at 100 × magnifications, and the disengaged or broken fragments were classified by their composition (*e.g.*, cobalt-chromium, acrylic resin,

Table 1
Fracture load values (N) registered at the left cantilever (LC) of the implant-supported hybrid prostheses.

Group	*n*	Mean	SD	Me	IQR	Min	Max
CC-A	5	1603.6 (a)	137.3	1650.0	170.0	1440.0	1778.0
CF-A	5	1546.8 (a)	58.0	1540.0	34.0	1470.0	1630.0
CF-R	5	799.4 (b)	93.0	840.0	130.0	674.0	893.0

Footnote: **CC-A (Group 1):** Acrylic-veneered Co-Cr implant-supported hybrid prostheses (HPs). **CF-A (Group 2):** Acrylic-coated carbon fiber HPs. **CF-R (Group 3):** Composite resin-coated carbon fiber HPs. **N:** Newton. **SD:** Standard deviation. **Me:** Median. **IQR:** Interquartile range. **Min:** Lowest fracture resistance (FR) value obtained in each group. **Max:** Highest FR value recorded in each group. In the third column, different letters indicate statistically significant differences ($p < 0.001$).

Table 2
Fracture load values (N) obtained at the anterior region (AR) of the implant-supported hybrid prostheses.

Group	*n*	Mean	SD	Me	IQR	Min	Max
CC-A	5	2148.0 (a)	154.2	2180.0	120.0	1890.0	2270.0
CF-A	5	1462.0 (b)	131.4	1480.0	120.0	1290.0	1640.0
CF-R	5	922.4 (c)	111.9	969.0	192.0	801.0	1040.0

Footnote: **CC-A (Group 1):** Acrylic-coated Co-Cr implant-supported hybrid prostheses (HPs). **CF-A (Group 2):** Acrylic-veneered carbon fiber HPs. **CF-R (Group 3):** Composite resin-coated carbon fiber HPs. **N:** Newton. **SD:** Standard deviation. **Me:** Median. **IQR:** Interquartile range. **Min:** Lowest fracture resistance (FR) value registered in each group. **Max:** Highest FR value recorded in each group. In the third column, different letters indicate statistically significant differences ($p < 0.001$).

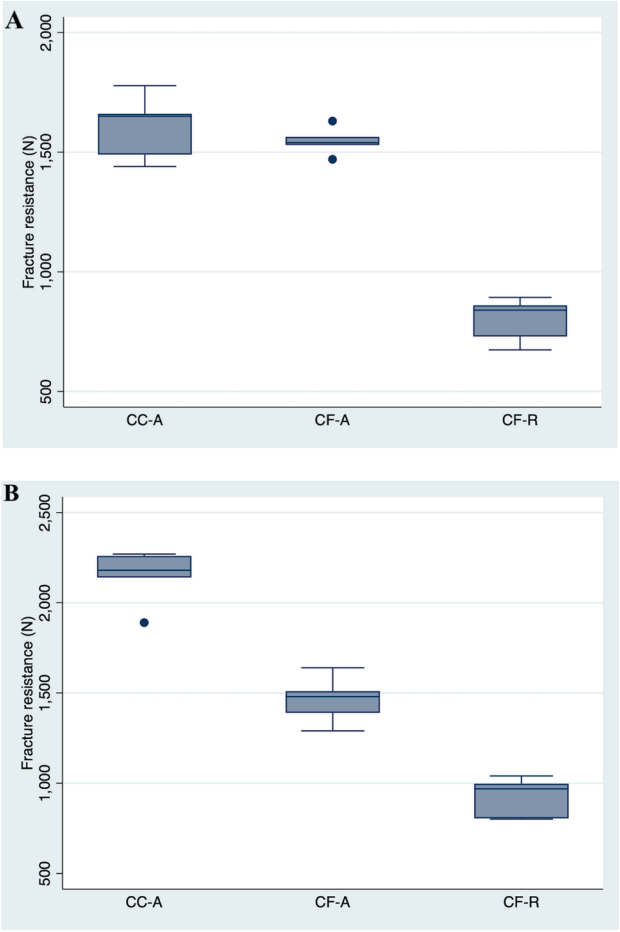

Fig. 2. Box plot of fracture resistance (FR). **A:** At the left cantilever (LC). **B:** At the anterior region (AR).

Table 3
Fracture resistance values (N) recorded at the LC and AR locations within each tested group.

Group	*n*	LC Mean (SD)	AR Mean (SD)	*p*-value
CC-A	5	1603.6 (137.3)	2148.0 (154.2)	<0.001
CF-A	5	1546.8 (58.0)	1462.0 (131.4)	0.223
CF-R	5	799.4 (93.0)	922.4 (111.9)	0.095

Footnote: **CC-A (Group 1):** Acrylic-veneered Co-Cr implant-supported hybrid prostheses (HPs). **CF-A (Group 2):** Acrylic-coated carbon fiber HPs. **CF-R (Group 3):** Composite resin-coated carbon fiber HPs. **LC:** Left cantilever. **AR:** Anterior region. **N:** Newton. **SD:** Standard deviation.

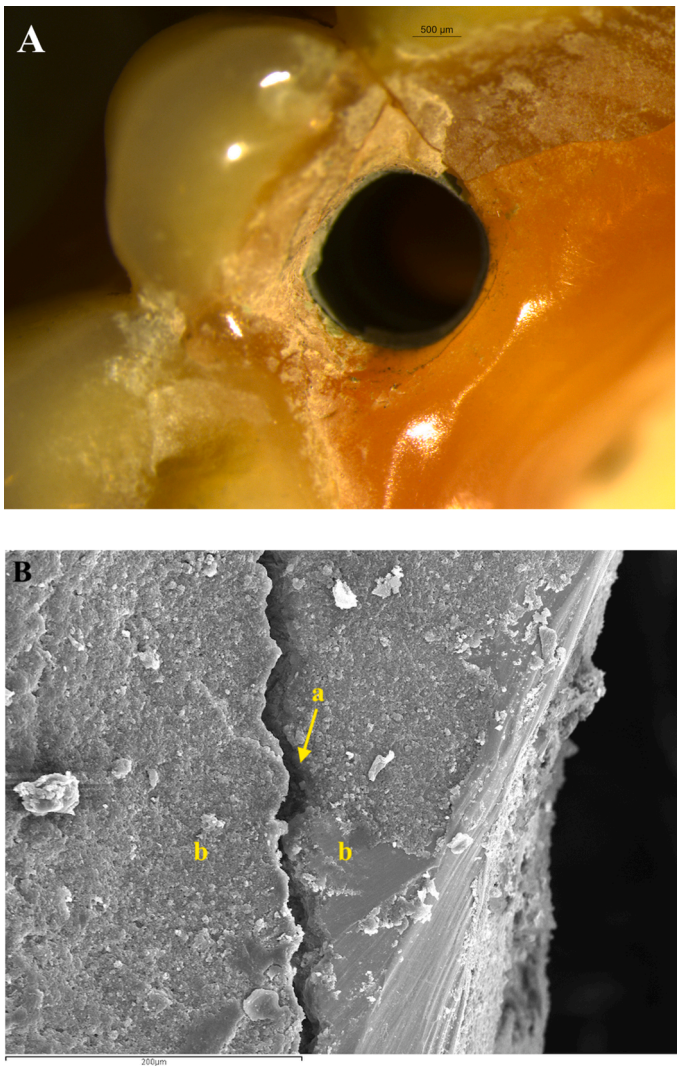

Fig. 3. A: Stereoscopic image (40 ×; bar 500 μm) of the CC-A_5 specimen. A superficial crack without chipping is noticeable at the access hole of the implant located next to the LC site. **B:** SEM magnification of this zone (250 ×; bar 200 μm). A fracture line ('a') within the thickness of the acrylic veneering ('b') is evident. The surface is slightly dotted with residues of the opaque paste.

carbon fiber, composite resin, luting material, etc.). After the assessment and classification of the fracture pattern, 300 × and 500 × magnifications were used to scan the surfaces for particles and material residues [36,41].

All the CC-A samples failed cohesively at both tested locations, showing fracture lines without debonding of the acrylic coating (Table 4, Fig. 3A). Cracks within the suprastructure and traces of the opaque paste were observed by SEM, which confirmed the cohesive failure (Table 4, Fig. 3B). A subtype of cohesive failure that consisted of crack lines without detachment of the veneering material, was identified at the LC site (40%) (Table 4, Fig. 3).

In the CF-A group, the predominant failure type was cohesive, both at the LC (100%), and the AR sites (60%) (Table 4). In these samples, the acrylic coating remained adhered to the mesostructure (Fig. 4A). At the LC, cracks were frequently detected around the distal implant connection (Fig. 4A). Less than half of the specimens in this group (40%) exhibited an adhesive fracture pattern at the AR location (Table 4, Fig. 4B), with a complete detachment of the acrylic veneering from the carbon-fiber mesostructure. The SEM-examination of these restorations revealed a clear gap with no remnants layering on the disengaged surfaces (Fig. 4B).

Most CF-R prostheses failed adhesively both at LC (100%) and AR sites (80%); the composite-resin veneering being detached from the underlying mesostructure (Table 4, Fig. 5A). Traces of adhesive or bonding materials were barely observed in this group. Only one specimen (20%) had vestiges of bonding residues at the AR site, which justified its classification as mixed failure (Table 4, Fig. 5B).

All HPs conserved their mesostructures intact after the bending test.

4. Discussion

Notwithstanding their proven durability, HPs frequently present biomechanical failures that include chipping, debonding of veneering material, detachment of artificial teeth, fractures of any component of the restoration, screw loosening, and peri-implant bone loss [5,8]. Undoubtedly, the cantilever length [19,26,44] and the combination of framework and coating materials [13] have important roles in resisting bending forces, knowing that the cantilevers are the weakest parts of a hybrid prosthesis [19,45]. The production of thinner, lighter CAD/CAM mesostructures has recently led to the use of rigid carbon fibers, as they may present similar rigidity to Co-Cr [16] and may allow enhanced union to the veneering material [28], which is expected to decrease chipping and fractures under occlusal loads.

However, research on the resistance of HPs fabricated with these new technologies is lacking [15,16,18], especially in cases of shortened dental arches [28,38]. This study involved a comparative assessment of fracture resistance (FR) and failure mode in maxillary short-cantilevered HPs made of three combinations of materials, via bending tests at two key locations (distal extension *vs.* anterior region). Our null hypothesis was rejected, as the HPs showed significantly different FR values and wide-ranging fracture patterns.

The CC-A and CF-A samples represented the most advantageous combinations of materials for maxillary HPs in terms of the FR of their 10-mm-long cantilevers. On the contrary, the CF-R prostheses yielded the significantly lowest FR values in the study, being the only group that did not attain the acceptable limit of 900 N at their LC [33] (Tables 1 and 3, Fig. 2A).

This could be due to the difference in acrylic resin's shock-absorbing capacity compared with composite resin, the latter presenting more

Table 4
Failure patterns observed after the bending tests within each group.

Group	*n*	Failure mode (LC)	Failure mode (AR)	Failure mode (LC+AR)	Failure site
CC-A	5	C (60%) C-Cr (40%)	C (100%)	C (80%) C-Cr (20%)	Acrylic resin coating / artificial teeth.
CF-A	5	C (100%)	C (60%) A (40%)	C (80%) A (20%)	Framework / chimney interface. Acrylic resin veneering.
CF-R	5	A (100%)	A (80%) M (20%)	A (90%) M (10%)	Framework / chimney interface. Composite resin veneering.

Footnote: **CC-A (Group 1):** Acrylic-veneered cobalt-chromium implant-supported hybrid prostheses (HPs). **CF-A (Group 2):** Acrylic-veneered carbon fiber HPs. **CF-R (Group 3):** Composite resin-coated carbon fiber HPs. **C:** Cohesive failure (within the veneering material). **C-Cr:** Subtype of cohesive failure consisting on the appearance of cracks without detachment of the suprastructure material. **A:** Adhesive failure (debonding of the coating material). **F:** Complete failure (which moreover includes framework fracture). **M**: Mixed failure (a combination of adhesive and cohesive modalities).

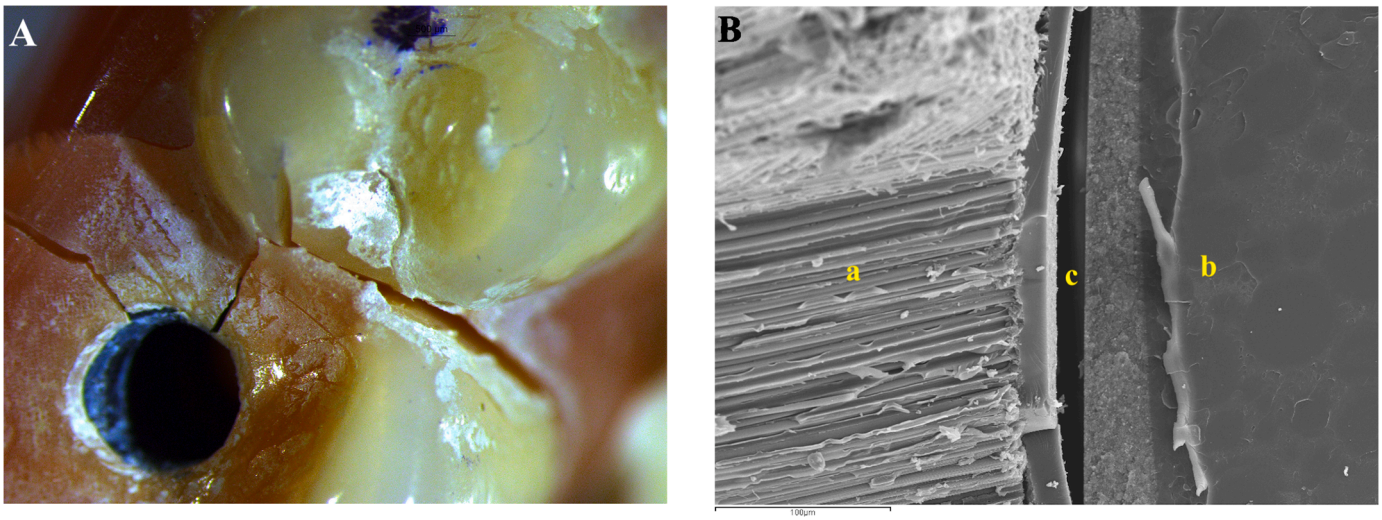

Fig. 4. **A:** Stereoscopic image (40 ×; bar 500 μm) of the CF-A_2 restoration taken at the LC site. Several fracture lines that involve the distal implant connection, are interconnected and propagated within both the artificial teeth and the acrylic gum. **B:** SEM micrograph (300 ×; bar 100 μm) of the CF-A_3 sample taken at the AR location. A microgap ('c') between the carbon-fiber mesostructure ('a') and the acrylic coating ('b') may be observed.

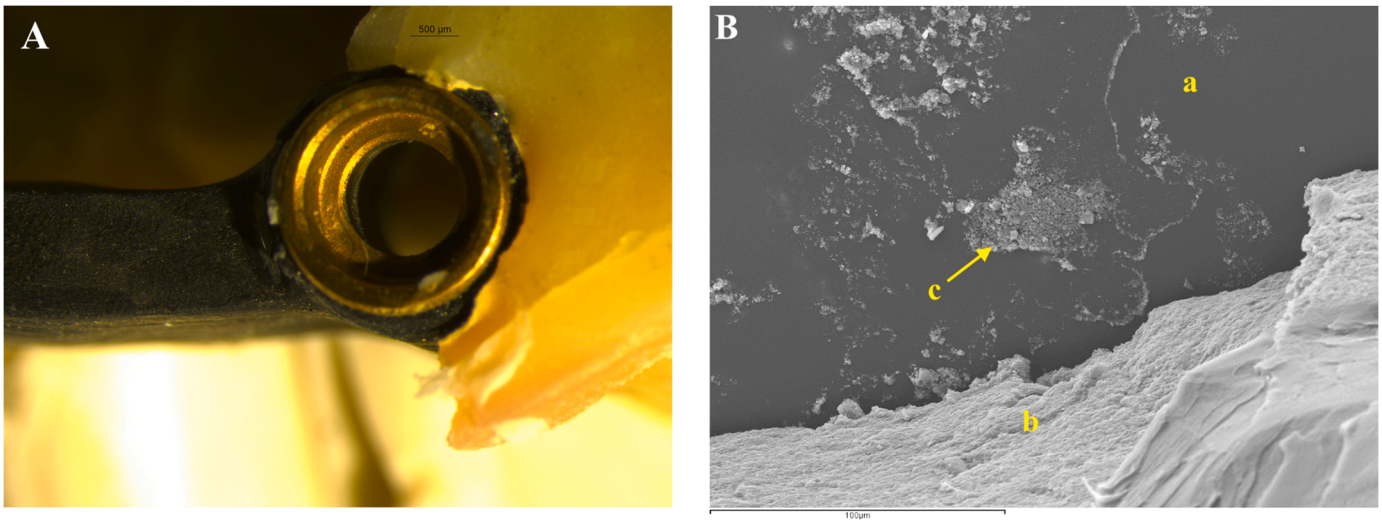

Fig. 5. **A:** Stereoscopic image (40 ×; bar 500 μm) of the CF-R_4 sample. A complete disjunction of the composite-resin veneering is visible at the LC site. **B:** SEM micrograph (500 ×; bar 100 μm) of the CF-R_1 prosthesis. The carbon-fiber mesostructure ('a'), the composite-resin coating ('b'), and some cement layers still bonded to the framework ('c'), may be observed.

rigidity [46,47]. In fact, the stiffer the prosthetic material (*i.e.,* having the higher elastic moduli), the greater the transmission of occlusal loads to the supporting implants is [47,48]. This unfavorable stress distribution can lead to fractured veneering material, also contributing to peri-implant bone loss [4,5]. On the contrary, acrylic resin's viscoelastic properties and low elastic moduli seem to dampen occlusal forces [13], thus reducing the stress concentration around the implant fixtures. Despite the frame composition, a shock-absorbing coating material such as acrylic [47,49] is crucial, as the loss of proprioception in implant rehabilitations propitiates increased loads [50].

Our findings cannot be rigorously contrasted with those of related investigations, as no previous bending tests have been carried out with 10-mm-long cantilevers of real HPs fabricated with the same combinations of mesostructure and veneering materials.

Despite the qualities attributed to carbon fibers [16,18,47], in the bending test developed with 13-mm-long cantilevers, none of the mesostructures constructed with this material reached a clinically acceptable threshold of 900 N [33] regardless of being coated with acrylic or composite resin [14]. In view of such findings, we decided to evaluate the mechanical behavior of the same combination of materials mimicking a shortened dental arch, thus comparing the resistance values of 10-mm-long extensions with those of intermediate sectors. According to a previous research, both cantilevers of the same prostheses were independently assessed [43]. As we justified in the Methods section, we used an even more accurate universal testing machine in the present study. Save the methodological differences, with the 10-mm-long cantilevers, the FR values of the HPs constructed with carbon-fiber mesostructures were more than double the FR values obtained with the 13-mm-long extensions within each group of coating materials. Moreover, with the 10-mm-long extensions, the FR of acrylic-veneered carbon-fiber frames was comparable to that of the Co-Cr gold standard (Tables 1 and 3, Fig. 2A) [14]. This result changes the paradigm, opening the door for acrylic-coated carbon fiber to be utilized for fabricating HPs with cantilevers up to 10 mm.

At the AR site, the CC-A prostheses achieved the significantly highest FR values, while the CF-R samples were the least resistant. The CF-A

restorations obtained intermediate values between those of the CC-A and CF-R samples, showing significant differences with both of them (Tables 2 and 3, Fig. 2B). The CF-R group was included in our study because composite coating may be clinically repaired, offering a good solution for esthetic failures of maxillary rehabilitations [51] thanks to the continuous advancement in bonding and composite technologies [52,53]. As always, our results cannot be rigorously analogised with those of the literature, as unrealistic specimens, different fiber-reinforced composites, and diverse laboratory fabrication techniques, testing methods, and analysed locations have been reported [17,18,54,55].

Disregarding the methodological differences, our conclusions are in line with those of Menini et al. [16], who suggested that carbon-fiber-reinforced composite structures might be a sufficient alternative to gold-alloy prosthetic frames after a bending test performed at an intermediate sector. These authors investigated manually constructed HPs with a 27-mm-long span, whereas our mesostructures were milled from prefabricated pure carbon-fiber disks, using a silicon mold to ensure that all samples had the same dimensions.

Except the CF-R specimens at the LC site, the overall FR values surpassed 900 N in all groups [33] (Tables 1-3). If we consider the threshold of 1000 N proposed by some authors on the basis that this is the limit of parafunctional forces [56,57], we would have to affirm that CF-R samples do not reach the minimum resistance values at any location (Tables 1-3). Even so, no carbon-fiber framework fractured after the bending test (Figs. 4A and 5A). Thus, the maximal bite force, which varies depending on gender [58,59], age [60], the presence of parafunctional habits [61,62], and the nature of the opposing arch [63,64], should influence the choice of carbon-fiber frames instead of metallic ones.

CF-A and CF-R samples did not demonstrate FR differences depending on the prosthesis' location. Conversely, the FR registered at the LC of the CC-A prostheses was significantly lower than that recorded at their AR (Table 3). This may be due to the higher rigidity of metal alloys when compared to carbon-fiber mesostructures [16]. While the stiffness of prosthetic frameworks is a key factor in even stress distribution to abutments and implants [13], the lower deformation capacity of metals, in addition to the force magnification that occurs at the cantilevers, may have made CC-A restorations more prone to mechanical failure [16,43]. In contrast, carbon-fiber frames are more resilient due to their higher elasticity [16].

As for the fracture patterns, all CC-A samples failed cohesively; fractures of the artificial teeth usually started from the occlusal surface (Fig. 3A), leading to a deeper damage (Fig. 3B). At the LC site, 40% of these HPs presented crack lines without acrylic detachment (Table 4, Fig. 3A). Agreeing with the literature, the distal implant connections were the most fragile areas in this group [43], showing fissures at the interface with the prosthesis (Fig. 3A). A cohesive failure type involving the distal connection was predominant in the CF-A group (Table 4, Fig. 4A). The greater elasticity of acrylic resin compared to composite, which is more rigid, may contribute to a more intense bond to the substrate, regardless of whether the mesostructure is made of metal or carbon fiber. Nonetheless, a low percentage of adhesive failures were recorded in this group, unlike what happened in the CC-A set (Table 4, Fig. 4B). Probably owing to the different elastic moduli of the framework and coating materials, most CF-R prostheses failed adhesively (Table 4, Fig. 5A), which is in accordance with previous findings [14,18]. Mixed failures occurred in minor proportion (Fig. 5B). Delamination, fractures, and chipping may be associated with the brittle nature [65] and unreliable union of the composite to the mesostructure. Hence, a standardised bonding protocol and improved laboratory methods must be implemented.

Further studies are needed before our findings are extrapolated to the clinical setting, because real restorations are subject to multidirectional occlusal forces and complex bio-thermo-mechanical conditions [36,66]. Many elements must be taken into account when the distribution of loads are evaluated (implant, abutment, degree of osseointegration, bone geometry, bone density, type of forces, prosthesis' connection, etc.). Implants tend to show greater stress concentrations at the cortical bone. This effect increases as the bone quality decreases (*i.e.,* as the difference in stiffness between cortical and trabecular areas increases) [67–69].

Given that the stress generated under loading may vary depending on the bone quality, density, and region, we have prevented confounding variables from interfering with our *in vitro* research by ruling out the influence of bone, and focusing on the prosthetic materials prior to carry out further clinical investigations. Actually, one study limitation was the fact that no synthetic material that replicates the alveolar bone was used to hold the implants in place, so that the lack of transmission of forces to the 'alveolar bone', may have somewhat contributed to the difficulty of composite-veneered carbon-fiber HPs to achieving the clinically acceptable FR values.

5. Conclusions

Within the limitations of this *in vitro* study, the following conclusions may be drawn:

1 For full-arch maxillary HPs with short cantilevers ($\leq$ 10 mm), acrylic-resin-veneered carbon-fiber mesostructures may be recommended, as their distal extensions achieved comparable FR values to those of acrylic-coated Co-Cr HPs. Composite-veneered carbon-fiber HPs are not an acceptable alternative for this purpose, as they were the only ones whose cantilevers did not exceed the minimum acceptable FR of 900 N.
2 When measuring the FR at intermediate locations (*i.e.,* the anterior region), all material combinations surpassed the FR of 900 N. Acrylic-coated Co-Cr HPs proved to be the most resistant, followed by acrylic-coated carbon-fiber restorations, which, in turn, were more resistant than composite-coated carbon-fiber HPs.
3 Regardless of their veneering material, carbon-fiber HPs displayed similar FR values at both tested sites (cantilever *vs.* anterior region).
4 All acrylic-resin-veneered Co-Cr HPs showed cohesive failures, often chipping without disengagement. Most HPs made of acrylic-coated carbon fiber failed cohesively. On the contrary, the main failure type among composite-coated carbon-fiber HPs was adhesive, which was the most critical fracture pattern.

Funding

This research did not receive any specific grant from funding agencies in the public, commercial, or not-for-profit sectors.

Declaration of competing interests

The authors declare that they have no known competing financial interests or personal relationships that could have appeared to influence the work reported in this paper.

Acknowledgments

To Tony Muscia (Procotech Dental Laboratory, Madrid, Spain), for the selflessly fabrication of the prostheses. To Prof. Pradíes (Complutense University of Madrid, U.C.M., Spain), for sharing with us the thermal cycling machine and the stereomicroscope of his research team. To Santiago Cano, of the Centre of Data Processing (Computing Service for Research Support of the U.C.M.), for his expert assistance with the statistical analysis. Finally, the first author would like to mention Doctor Tigran Haroyan Ghazaryan, for his wise advice and support.

References

[1] M. Menéndez-Collar, M.A. Serrera-Figallo, P. Hita-Iglesias, R. Castillo-Oyagüe, J. C. Casar-Espinosa, A. Gutiérrez-Corrales, J.L. Gutiérrez-Perez, D. Torres-Lagares, Straight and tilted implants for supporting screw-retained full-arch dental prostheses in atrophic maxillae: a 2-year prospective study, Med. Oral Patol. Oral Cir. Bucal 23 (2018) e733–e741, https://doi.org/10.4317/medoral.22459.

[2] G. Priest, J. Smith, M.G. Wilson, Implant survival and prosthetic complications of mandibular metal-acrylic resin implant complete fixed dental prostheses, J. Prosthet. Dent. 111 (2014) 466–475, https://doi.org/10.1016/j.prosdent.2013.07.027.

[3] G.O. Gallucci, C.B. Doughtie, J.W. Hwang, J.P. Fiorellini, H.P. Weber, Five-year results of fixed implant-supported rehabilitations with distal cantilevers for the edentulous mandible, Clin. Oral. Implants Res. 20 (2009) 601–607, https://doi.org/10.1111/j.1600-0501.2008.01699.x.

[4] C. Drago, Ratios of cantilever lengths and anterior-posterior spreads of definitive hybrid full-arch, screw-retained prostheses: results of a clinical study, J. Prosthodont. 27 (2018) 402–408, https://doi.org/10.1111/jopr.12519.

[5] B. Rangert, P.H. Krogh, B. Langer, N. Van Roekel, Bending overload and implant fracture: a retrospective clinical analysis, Int. J. Oral Maxillofac. Implants 10 (1995) 326–334.

[6] K.S. Kim, Y.L. Kim, J.M. Bae, H.W. Cho, Biomechanical comparison of axial and tilted implants for mandibular full-arch fixed prostheses, Int. J. Oral Maxillofac. Implants 26 (2011) 976–984.

[7] A.M. Rodriguez, S.A. Aquilino, P.S. Lund, Cantilever and implant biomechanics: a review of the literature, Part 2, J. Prosthodont. 3 (1994) 114–118, https://doi.org/10.1111/j.1532-849x.1994.tb00138.x.

[8] L. Walter, G. Greenstein, Utility of measuring anterior-posterior spread to determine distal cantilever length off a fixed implant-supported full-arch prosthesis, J. Am. Dent. Assoc. 151 (2020) 790–795, https://doi.org/10.1016/j.adaj.2020.06.016.

[9] C.E. English, Critical A-P spread, Implant. Soc. 1 (1990) 2–3.

[10] W. Daudt Polido, T. Aghaloo, T.W. Emmett, T.D. Taylor, D. Morton, Number of implants placed for complete-arch fixed prostheses: a systematic review and meta-analysis, Clin. Oral Implants Res. 29 (Suppl 16) (2018) 154–183, https://doi.org/10.1111/clr.13312.

[11] F. de C.P. Gonçalves, M. Amaral, A.L.S. Borges, L.F.M. Gonçalves, T.J. de A. Paes-Junior, Fracture load of complete-arch implant-supported prostheses reinforced with nylon-silica mesh: an *in vitro* study, J. Prosthet. Dent. 119 (2018) 606–610, https://doi.org/10.1016/j.prosdent.2017.05.018.

[12] G. Sagat, S. Yalcin, B.A. Gultekin, E. Mijiritsky, Influence of arch shape and implant position on stress distribution around implants supporting fixed full-arch prosthesis in edentulous maxilla, Implant Dent 19 (2010) 498–508, https://doi.org/10.1097/ID.0b013e3181fa4267.

[13] R. Skalak, Biomechanical considerations in osseointegrated prostheses, J. Prosthet. Dent. 49 (1983) 843–848, https://doi.org/10.1016/0022-3913(83)90361-x.

[14] E. Haroyan-Darbinyan, M. Romeo-Rubio, J. Río-Highsmith, C.D. Lynch, R. Castillo-Oyagüe, Fracture resistance of cantilevered full-arch implant-supported hybrid prostheses with carbon fiber frameworks after thermal cycling, J. Dent. 116 (2022), 103902, https://doi.org/10.1016/j.jdent.2021.103902.

[15] F. Pera, P. Pesce, F. Solimano, T. Tealdo, P. Pera, M. Menini, Carbon fibre *versus* metal framework in full-arch immediate loading rehabilitations of the maxilla - a cohort clinical study, J. Oral Rehabil. 44 (2017) 392–397, https://doi.org/10.1111/joor.12493.

[16] M. Menini, P. Pesce, F. Pera, F. Barberis, A. Lagazzo, L. Bertola, P. Pera, Biological and mechanical characterization of carbon fiber frameworks for dental implant applications, Mater. Sci. Eng. C. Mater. Biol. Appl. 70 (2017) 646–655, https://doi.org/10.1016/j.msec.2016.09.047.

[17] P. Pesce, A. Lagazzo, F. Barberis, L. Repetto, F. Pera, D. Baldi, M. Menini, Mechanical characterisation of multi *vs.* uni-directional carbon fiber frameworks for dental implant applications, Mater. Sci. Eng. C. Mater. Biol. Appl. 102 (2019) 186–191, https://doi.org/10.1016/j.msec.2019.04.036.

[18] M. Menini, F. Pera, F. Barberis, G. Rosenberg, F. Bagnascoa, P. Pesce, Evaluation of adhesion between carbon fiber frameworks and esthetic veneering materials, Int. J. Prosthodont. 31 (2018) 453–455, https://doi.org/10.1016/j.msec.2019.04.036.

[19] J.L. Shackleton, L. Carr, J.C. Slabbert, P.J. Becker, Survival of fixed implant-supported prostheses related to cantilever lengths, J. Prosthet. Dent. 71 (1994) 23–26, https://doi.org/10.1016/0022-3913(94)90250-x.

[20] Y.J. Kim, J. Henkin, Micro-computed tomography assessment of human alveolar bone: bone density and three-dimensional micro-architecture: micro-CT assessment of human alveolar bone, Clin. Implant Dent. Relat. Res. 17 (2015) 307–313, https://doi.org/10.1111/cid.12109.

[21] I. Naert, M. Quirynen, D. van Steenberghe, P. Darius, A study of 589 consecutive implants supporting complete fixed prostheses. Part II: prosthetic aspects, J. Prosthet. Dent. 68 (1992) 949–956, https://doi.org/10.1016/0022-3913(92)90557-q.

[22] B. Rangert, T. Jemt, L. Jörneus, Forces and moments on Branemark implants, Int. J. Oral Maxillofac. Implants 4 (1989) 241–247.

[23] R.M. Watson, D.M. Davis, G.H. Forman, T. Coward, Considerations in design and fabrication of maxillary implant-supported prostheses, Int. J. Prosthodont. 4 (1991) 232–239.

[24] E.J. Rasmussen, Alternative prosthodontic technique for tissue-integrated prostheses, J. Prosthet. Dent. 57 (1987) 198–204, https://doi.org/10.1016/0022-3913(87)90147-8.

[25] A. Shireen, S. Ara, Odontometric analysis of permanent maxillary first molar in gender determination, J. Forensic Dent. Sci. 8 (2016) 145, https://doi.org/10.4103/0975-1475.195120.

[26] C. Drago, Cantilever lengths and anterior-posterior spreads of interim, acrylic resin, full-arch screw-retained prostheses and their relationship to prosthetic complications, J. Prosthodont. 26 (2017) 502–507, https://doi.org/10.1111/jopr.12426.

[27] S. Liang, Q. Zhang, D.J. Witter, Y. Wang, N.H. Creugers, Effects of removable dental prostheses on masticatory performance of subjects with shortened dental arches: a systematic review, J. Dent. 43 (2015) 1185–1194, https://doi.org/10.1016/j.jdent.2015.05.008.

[28] A.S. Abdulghani, S.B. Elhag, Shortened dental arch as a solution for maxillary sinus proximity in dental implant restoration, Clin. Case Rep. 5 (2017) 782–786, https://doi.org/10.1002/ccr3.923.

[29] K. Fueki, Y. Igarashi, Y. Maeda, K. Baba, K. Koyano, K. Sasaki, Y. Akagawa, T. Kuboki, S. Kasugai, N.R. Garrett, Effect of prosthetic restoration on masticatory function in patients with shortened dental arches: a multicentre study, J. Oral Rehabil. 43 (2016) 534–542, https://doi.org/10.1111/joor.12387.

[30] T. Kanno, G.E. Carlsson, A review of the shortened dental arch concept focusing on the work by the Käyser/Nijmegen group: a review of the shortened dental arch concept, J. Oral Rehabil. 33 (2006) 850–862, https://doi.org/10.1111/j.1365-2842.2006.01625.x.

[31] A. Sertgöz, S. Güvener, Finite element analysis of the effect of cantilever and implant length on stress distribution in an implant-supported fixed prosthesis, J. Prosthet. Dent. 76 (1996) 165–169, https://doi.org/10.1016/s0022-3913(96)90301-7.

[32] R.Tiossi R, É.A. Gomes, A.C.L. Faria, R.C.S. Rodrigues, R.F. Ribeiro, Biomechanical behavior of titanium and zirconia frameworks for implant-supported full-arch fixed dental prosthesis, Clin. Implant Dent. Relat. Res. 19 (2017) 860–866, https://doi.org/10.1111/cid.12525.

[33] V.F. Ferrario, C. Sforza, A. Colombo, V. Ciusa, An electromyographic investigation of masticatory muscles symmetry in normo-occlusion subjects, J. Oral Rehabil. 27 (2000) 33–40, https://doi.org/10.1046/j.1365-2842.2000.00490.x.

[34] C.C. Serdar, M. Cihan, D. Yücel, M.A. Serdar, Sample size, power and effect size revisited: simplified and practical approaches in pre-clinical, clinical and laboratory studies, Biochem. Med. (Zagreb) 31 (2021), 010502, https://doi.org/10.11613/BM.2021.010502.

[35] R.C. Oyagüe, M.I. Sánchez-Jorge, A. Sánchez Turrión, Evaluation of fit of zirconia posterior bridge structures constructed with different scanning methods and preparation angles, Odontology 98 (2010) 170–172, https://doi.org/10.1007/s10266-010-0122-7.

[36] R. Castillo Oyagüe, M.I. Sánchez-Jorge, A. Sánchez Turrión, Influence of CAD/CAM scanning method and tooth-preparation design on the vertical misfit of zirconia crown copings, Am. J. Dent. 23 (2010) 341–346.

[37] E.T. Giampaolo, J.H. Jorge, A.L. Machado, A.C. Pavarina, C.E. Vergani, Effect of thermal cycling on microleakage between hard chairside relines and denture base acrylic resins, Gerodontology 28 (2011) 121–126, https://doi.org/10.1111/j.1741-2358.2009.00332.x.

[38] Y. Maeda, M. Sogo, S. Tsutsumi, Efficacy of a posterior implant support for extra shortened dental arches: a biomechanical model analysis, J. Oral Rehabil. 32 (2005) 656–660, https://doi.org/10.1111/j.1365-2842.2005.01478.x.

[39] M. Rosentritt, A. Rembs, M. Behr, S. Hahnel, V. Preis, *In vitro* performance of implant-supported monolithic zirconia crowns: influence of patient-specific tooth-coloured abutments with titanium adhesive bases, J. Dent. 43 (2015) 839–845, https://doi.org/10.1016/j.jdent.2015.04.011.

[40] T. Albrecht, A. Kirsten, H.F. Kappert, H. Fischer, Fracture load of different crown systems on zirconia implant abutments, Dent Mater 27 (2011) 298–303, https://doi.org/10.1016/j.dental.2010.11.005.

[41] R. Castillo-de-Oyagüe, A. Sánchez-Turrión, J.F. López-Lozano, A. Albaladejo-Martínez, D. Torres-Lagares, J. Montero, M.J. Suárez, Vertical misfit of laser-sintered and vacuum-cast implant-supported crown copings luted with definitive and temporary luting agents, Med. Oral Patol. Oral Cir. Bucal 17 (2012) e610–e617, https://doi.org/10.4317/medoral.17997.

[42] T.R. Vetter, Fundamentals of research data and variables: the devil is in the details, Anesthesia & Analgesia 124 (2017) 1375–1380, https://doi.org/10.1213/ANE.0000000000002370.

[43] J. Goldberg, G. Ronaghi, J.H. Phark, S. Jivraj, W. Chee, Force-to-failure of a simulated implant-supported complete fixed dental prosthesis reinforced with glass fiber, J. Prosthet. Dent. 118 (2017) 172–176, https://doi.org/10.1016/j.prosdent.2016.11.010.

[44] B.A. Purcell, E.A. McGlumphy, B. Yilmaz, J.A. Holloway, F.M. Beck, Anteroposterior spread and cantilever length in mandibular metal-resin implant-fixed complete dental prostheses: a 7- to 9-year analysis, Int. J. Prosthodont. 28 (2015) 512–518, https://doi.org/10.11607/ijp.4172.

[45] G.A. Zarb, A. Schmitt, The longitudinal clinical effectiveness of osseointegrated dental implants: the Toronto Study. Part II: the prosthetic results, J. Prosthet. Dent. 64 (1990) 53–61, https://doi.org/10.1016/0022-3913(90)90153-4.

[46] K. Masouras, N. Silikas, D.C. Watts, Correlation of filler content and elastic properties of resin-composites, Dent. Mater. 24 (2008) 932–939, https://doi.org/10.1016/j.dental.2007.11.007.

[47] M. Menini, E. Conserva, T. Tealdo, M. Bevilacqua, F. Pera, A. Signori, P. Pera, Shock absorption capacity of restorative materials for dental implant prostheses: an *in vitro* study, Int. J. Prosthodont. 26 (2013) 549–556, https://doi.org/10.11607/ijp.3241.

[48] S.E. Gracis, J.I. Nicholls, J.D. Chalupnik, R.A. Yuodelis, Shock-absorbing behavior of five restorative materials used on implants, Int. J. Prosthodont. 4 (1991) 282–291.
[49] R. Skalak, Biomechanical considerations in osseointegrated prostheses, J. Prosthet. Dent. 49 (1983) 843–848, https://doi.org/10.1016/0022-3913(83)90361-x.
[50] K. Koyano, D. Esaki, Occlusion on oral implants: current clinical guidelines, J. Oral Rehabil. 42 (2015) 153–161, https://doi.org/10.1111/joor.12239.
[51] E.A. Bonfante, M. Suzuki, R. Hirata, G. Bonfante, V.P. Fardin, P.G. Coelho, Resin composite repair for implant-supported crowns: repair of implant-supported crowns, J. Biomed. Mater. Res. 105 (2017) 1481–1489, https://doi.org/10.1002/jbm.b.33683.
[52] A.S. Gilmour, P. Evans, L.D. Addy, Attitudes of general dental practitioners in the UK to the use of composite materials in posterior teeth, Br. Dent. J. 202 (2007) 32, https://doi.org/10.1038/bdj.2007.472.
[53] R. Castillo-de Oyagüe, C. Lynch, R. McConnell, N. Wilson, Teaching the placement of posterior resin-based composite restorations in Spanish dental schools, Med. Oral Patol. Oral Cir. Bucal 17 (2012) e661–e668, https://doi.org/10.4317/medoral.17656.
[54] E.T.P. Bergamo, T.M.C. Bastos, A.C.O. Lopes, E.N.S. de Araujo Júnior, P.G. Coelho, E.B. Benalcazar Jalkh, A. Zahoui, E.A. Bonfante, Physicochemical and mechanical characterization of a fiber-reinforced composite used as frameworks of implant-supported prostheses, Dent. Mater. 37 (2021) e443–e453, https://doi.org/10.1016/j.dental.2021.03.014.
[55] M.M. Rayyan, J. Abdallah, L.G. Segaan, E.A. Bonfante, E. Osman, Static and fatigue loading of veneered implant-supported fixed dental prostheses, J. Prosthodont. 29 (2020) 679–685, https://doi.org/10.1111/jopr.13173.
[56] J. Schmitt, S. Holst, M. Wichmann, S. Reich, M. Gollner, J. Hamel, Zirconia posterior fixed partial dentures: a prospective clinical 3-year follow-up, Int. J. Prosthodont. 22 (2009) 597–603.
[57] C. López-Suárez, R. Castillo-Oyagüe, V. Rodríguez-Alonso, C.D. Lynch, M.J. Suárez-García, Fracture load of metal-ceramic, monolithic, and bi-layered zirconia-based posterior fixed dental prostheses after thermo-mechanical cycling, J. Dent. 73 (2018) 97–104, https://doi.org/10.1016/j.jdent.2018.04.012.
[58] S. Levartovsky, G. Peleg, S. Matalon, I. Tsesis, E. Rosen, Maximal bite force measured via digital bite force transducer in subjects with or without dental implants—a pilot study, Appl. Sci. 12 (2022) 1544, https://doi.org/10.3390/app12031544.
[59] M.K. Al-Omiri, M.G. Sghaireen, M.M. Alhijawi, I.A. Alzoubi, C.D. Lynch, E. Lynch, Maximum bite force following unilateral implant-supported prosthetic treatment: within-subject comparison to opposite dentate side, J. Oral Rehabil. 41 (2014) 624–629, https://doi.org/10.1111/joor.12174.
[60] M. Palinkas, M.S.P. Nassar, F.A. Cecílio, M.Semprini S.Siéssere, J.P. Machado-de-Sousa, J.E. Hallak, S.C. Regalo, Age and gender influence on maximal bite force and masticatory muscles thickness, Arch. Oral Biol. 55 (2010) 797–802, https://doi.org/10.1016/j.archoralbio.2010.06.016.
[61] B.R. Chrcanovic, J. Kisch, T. Albrektsson, A. Wennerberg, Bruxism and dental implant treatment complications: a retrospective comparative study of 98 bruxer patients and a matched group, Clin. Oral Implants Res. 28 (2017) e1–e9, https://doi.org/10.1111/clr.12844.
[62] B.R. Chrcanovic, J. Kisch, C. Larsson, Retrospective evaluation of implant-supported full-arch fixed dental prostheses after a mean follow-up of 10 years, Clin. Oral Implants Res. 32 (2020) 634–645, https://doi.org/10.1111/clr.13600.
[63] F. Müller, M. Hernandez, L. Grütter, L. Aracil-Kessler, D. Weingart, M. Schimmel, Masseter muscle thickness, chewing efficiency and bite force in edentulous patients with fixed and removable implant-supported prostheses: a cross-sectional multicenter study: masseter muscle thickness and bite force, Clin. Oral Implants Res. 23 (2012) 144–150, https://doi.org/10.1111/j.1600-0501.2011.02213.x.
[64] C. Göthberg, T. Bergendal, T. Magnusson, Complications after treatment with implant-supported fixed prostheses: a retrospective study, Int. J. Prosthodont. 16 (2003) 201–207.
[65] N.M. Ajaj-Alkordy, M.H. Alsaadi, Elastic modulus and flexural strength comparisons of high-impact and traditional denture base acrylic resins, Saudi Dent. J. 26 (2014) 15–18, https://doi.org/10.1016/j.sdentj.2013.12.005.
[66] A.A. Xible, R.R. de Jesus Tavarez, R. de Araujo Cdos, W.C. Bonachela, Effect of silica coating and silanization on flexural and composite-resin bond strengths of zirconia posts: an *in vitro* study, J. Prosthet. Dent. 95 (2006) 224–229, https://doi.org/10.1016/j.prosdent.2005.12.010.
[67] D. Bozkaya, S. Muftu, A. Muftu, Evaluation of load transfer characteristics of five different implants in compact bone at different load levels by finite elements analysis, J. Prosthet. Dent. 92 (2004) 523–530, https://doi.org/10.1016/j.prosdent.2004.07.024.
[68] F. Azcarate-Velázquez, R. Castillo-Oyagüe, L.G. Oliveros-López, D. Torres-Lagares, Á.J. Martínez-González, A. Pérez-Velasco, C.D. Lynch, J.L. Gutiérrez-Pérez, M.Á. Serrera-Figallo, Influence of bone quality on the mechanical interaction between implant and bone: a finite element analysis, J. Dent. 88 (2019), 103161, https://doi.org/10.1016/j.jdent.2019.06.008.
[69] F. Cozzolino, D. Apicella, G. Wang, A. Apicella, R. Sorrentino, Implant-to-bone force transmission: a pilot study for *in vivo* strain gauge measurement technique, J. Mech. Behav. Biomed. Mater. 90 (2019) 173–181, https://doi.org/10.1016/j.jmbbm.2018.10.014.